Chem

Article

Cooperative hydrogenation catalysis at a constrained gallylene-nickel(0) interface

Graphical abstract

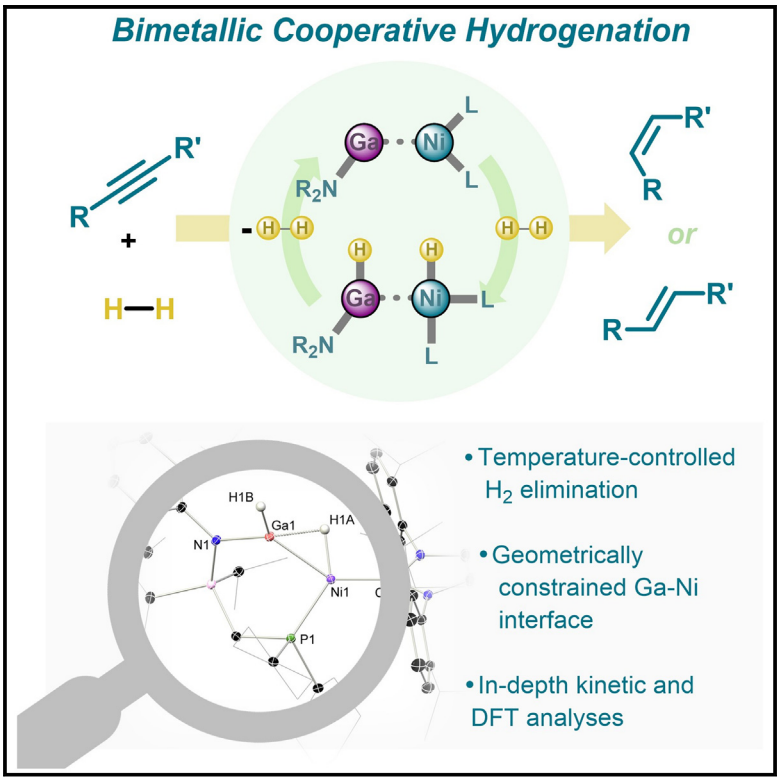

Highlights

- Geometric constraint at a bimetallic interface for cooperative, reversible H_2 scission
- Earth-abundant alkyne semi-hydrogenation catalyst utilizing Ga and Ni in concert
- Key insights via kinetic analysis of hydrogen elimination and alkyne hydrogenation
- Unexplored mechanisms in H_2 transfer and alkene isomerization via bimetallic cooperativity

Authors

Till L. Kalkuhl, Israel Fernández, Terrance J. Hadlington

Correspondence

terrance.hadlington@tum.de

In brief

The development of efficient and sustainable catalytic systems is of continuous importance in moving toward a circular chemical economy. This work demonstrates the power of cooperativity, whereby two Earth-abundant elements (viz., Ga and Ni) can work in concert to achieve thermo-neutral hydrogen activation. This is extended to the well-defined and selective catalytic semi-hydrogenation of alkynes, an important alkyne functionalization reaction, via a previously unknown mechanistic pathway that involves both metal centers in the bimetallic catalyst.

Kalkuhl et al., 2025, Chem *11*, 102349
April 10, 2025

https://doi.org/10.1016/j.chempr.2024.10.016

CellPress

Chem

CellPress
OPEN ACCESS

Article

Cooperative hydrogenation catalysis at a constrained gallylene-nickel(0) interface

Till L. Kalkuhl,[1] Israel Fernández,[2] and Terrance J. Hadlington[1,3,*]

[1]Fakultät für Chemie, School of Natural Sciences, TU München, Lichtenberg Strasse 4, 85749 Garching, Germany

[2]Departamento de Química Orgánica I, Facultad de Ciencias Químicas and Centro de Innovación en Química Avanzada (ORFEO-CINQA), Universidad Complutense de Madrid, Madrid, Spain

[3]Lead contact

*Correspondence: terrance.hadlington@tum.de

https://doi.org/10.1016/j.chempr.2024.10.016

THE BIGGER PICTURE A central challenge in next-generation catalysis is the utilization of Earth-abundant elements as catalysts for waste-free transformations. Though heterogeneous systems are well developed in this space, mechanistic understanding is poor due to challenges with *in operando* characterization of those systems. Hetero-multimetallic homogeneous systems can be actively employed here to amplify catalytic activity while gaining significant insights from the suite of characterization methods available under homogeneous solution-state conditions. Here, we draw inspiration from heterogeneous hydrogenation catalysts in the development of a geometrically constrained gallylene-nickel complex. This discrete molecular system can readily cleave dihydrogen, in forming hydrido-gallyl and hydrido-nickel moieties, reminiscent of spatially well-defined multi-site hydride formation in heterogeneous systems. The GaNi-hydride complex demonstrates temperature-controlled dihydrogen activation, extruding H_2 above 50°C, and can also catalytically transfer the activated dihydrogen to alkynes, selectively forming either (*Z*)- or (*E*)-alkenes depending on reaction conditions. The molecular nature of this system allows for in-depth kinetic analysis of hydrogen elimination and hydrogen transfer processes. These insights, combined with quantum chemical calculations, demonstrate that the catalytic process proceeds via a dual-center cooperative mechanism involving both Ga and Ni, featuring an initial hydride transfer from Ga to the alkyne substrate. Moreover, (*Z*)-to-(*E*) alkene isomerization is shown to proceed via a closely related second-sphere, Ga-centered hydrogen abstraction mechanism, in contrast to well-established mechanisms that proceed via classical β-hydride elimination. This demonstrates the power of bimetallic, cooperative catalysis, which we envisage will open pathways to further unprecedented reactive processes and mechanisms.

SUMMARY

The discovery of unique mechanisms in 3*d* metal catalysis is of paramount importance in utilizing these Earth-abundant metals in place of scarce precious metals. Inspired by the Horiuti-Polanyi mechanism at play in heterogeneous hydrogenation catalysts, we describe a bimetallic molecular catalyst that can selectively semi-hydrogenate alkynes via a ligand-to-substrate hydride transfer mechanism. This mimics established heterogeneous mechanisms in which remote surface-bound hydride ligands undergo a similar reactive process. This is achieved through the development of a chelate-constrained gallium(I) ligand, which operates in concert with nickel(0) to (reversibly) cleave H_2, generating a [GaNi] 1,2-dihydride complex that is found to be the resting state in the catalytic process. This discovery takes steps toward utilizing non-innocent low-valent group 13 centers in effective cooperative catalysis, opening new mechanistic pathways that may aid in employing Earth-abundant metals in key catalytic transformations.

INTRODUCTION

Catalytic processes that achieve the transfer of H_2 to a C–C triple bond are of central importance in chemical synthesis, presenting a sustainable, zero-waste method for alkyne functionalization.[1] Due to the particular utility of alkyne semi-hydrogenation in selectively accessing (*Z*)- or (*E*)-alkenes,[2] the development of efficient heterogeneous catalysts that can promote this transformation has been a key focus in applied settings.[3,4] Classical systems utilize Pd,[5,6] as well as other noble metals, whereby

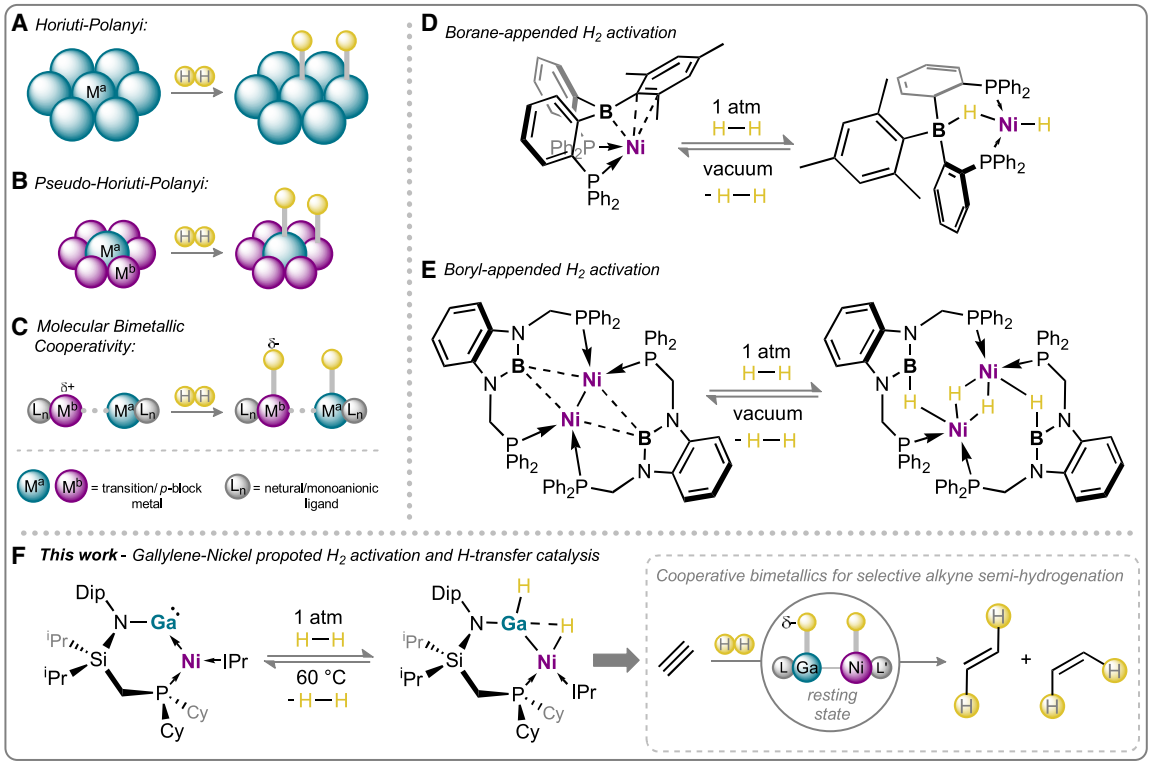

Figure 1. A comparison of bimetallic dihydrogen activation in hetero- and homogeneous alkyne hydrogenation catalysts, and our work toward bimetallic cooperativity in a molecular Ga^{I}-Ni^{0} system

(A) The well-established heterogeneous Horiuti-Polanyi mechanism for homolytic H_2 scission.

(B) The heterogeneous pseudo-Horiuti-Polanyi mechanism for heterolytic H_2 scission.

(C) Extending the pseudo-Horiuti-Polanyi mechanism to bimetallic homogeneous systems.

(D) and (E) Examples of group 13 element-assisted H_2 scission in their Ni complexes.

(F) Our work toward utilizing the low-valent group 13–nickel(0) interface for reversible H_2 scission and the well-defined cooperative semi-hydrogenation of alkynes at a bimetallic interface.

site-isolation (e.g., by "poisoning") is required to drive selectivity for semi-hydrogenation vs. full hydrogenation,[4] due to the importance of single-atom metal sites, which readily dissociate alkene products, circumventing over-hydrogenation.[7] Numerous materials have been developed to utilize more abundant, sustainable elements for this transformation,[4] leading to a plethora of *p*-block element–3*d*-transition metal materials that can selectively hydrogenate alkynes to alkenes under non-forcing conditions. Specifically, [FeGa], [NiGa], and [NiAl] alloys have demonstrated that the group 13 elements are highly proficient in this setting,[8–10] as an important shift away from Pd-derived catalysts. Heterogeneous alkene hydrogenation catalysts are well known to operate via the (pseudo) Horiuti-Polanyi mechanism,[4,11–14] whereby dihydrogen undergoes scission in the formation of surface hydrides (Figures 1A and 1B), which are ultimately transferred to surface-coordinated alkynes. This constitutes a bi- or poly-metallic hydrogenation mechanism, from which we can draw inspiration for molecular homogeneous catalysis (Figure 1C). Indeed, molecular heavier *d*-block bimetallics reported by Mankad et al. have demonstrated utility as alkyne semi-hydrogenation catalysts, proposed to operate via cooperative H_2 activation in forming intermolecular hydride species that work in concert to affect selective (*E*)-alkene formation.[15,16] Further examples of homo- and hetero-bimetallic systems have been reported that catalyze this process,[17,18] including MOF (metal-organic framework)-supported examples, which can affect the selective semi-hydrogenation of alkynes through cooperative mechanisms.[19–22]

Homogenous catalysts based upon abundant 3*d* metals have been a key focal point in the activation of H_2 and subsequent transfer to unsaturated substrates, as a move away from noble metals.[2,23,24] Cooperativity has played a key role in establishing such systems[21,25–27]; numerous catalysts are now known that feature proton acceptor ligands, which mitigate a formal oxidative addition/reductive elimination mechanism.[24,28] Redox-innocent Lewis acid ligands have also been employed as both spectators and hydride acceptors (Figure 1D),[22,29–32] which are known to amplify the catalytic efficiency of these systems. Anionic boron (i.e., boryl) ligands have been shown to also effect the activation of dihydrogen in TM complexes (Figure 1E) and further effect the catalytic hydrogenation of alkynes.[33] Still, in all described systems, a terminal ligand-centered hydride is not formed, and a broad exploration of catalytic efficacy in this regard has thus not been reported to date.

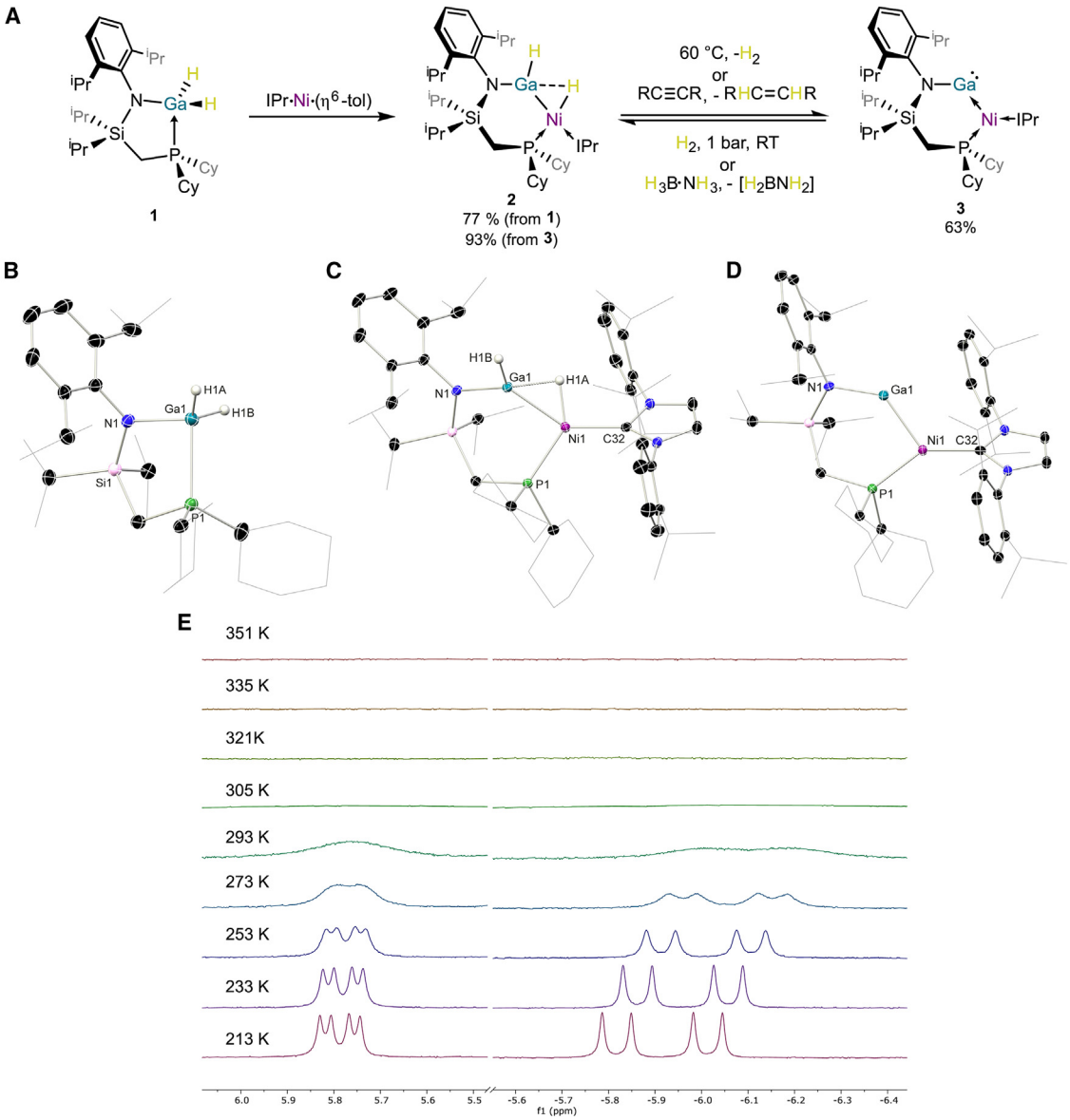

Figure 2. Accessing a gallylene-nickel(0) complex through H_2 expulsion from gallane

(A) The oxidative addition of phosphine-functionalized gallane **1** to nickel(0), forming **2**, and subsequent H_2 elimination or H_2 transfer.

(B) The molecular structure of **1**.

(C) The molecular structure of **2**.

(D) The molecular structure of **3**.

(E) Variable temperature ^{1}H NMR spectra of **2** in the range 213–351 K, indicative of signal broadening and eventual H_2 loss.

Our central goal in this study was to access a redox non-innocent, electropositive metallo-ligand that could affect the "molecular" Horiuti-Polanyi activation of dihydrogen. Indeed, related Al-Fe systems recently reported by Crimmin et al. demonstrate a significant amplification in bond activation capacity through bimetallic cooperativity,[34–36] while the groups of both Walensky and Fischer have demonstrated the bimetallic activation of H_2 in molecular U-Al species and soluble [NiGa] clusters, respectively.[37,38] We targeted highly electrophilic σ-donor ligands utilizing a group 13 element(I) center, built into a chelating ligand framework, to mimic the active sites of the aforementioned heterogeneous semi-hydrogenation catalysts. Such a system, with a strongly electrophilic ligand center, may benefit catalysis on two fronts: (1) the non-innocent ligand center allows for mimicry of the described heterogeneous hydrogenation mechanism, whereby H_2 activation generates a second-sphere, ligand-bound hydride ligand, which is subsequently transferred to a metal-bound unsaturated C–C bond and (2) the highly electropositive ligand center, which bares two vacant *p*-orbitals, may drive reductive elimination from a 3*d*-metal center. Herein, we

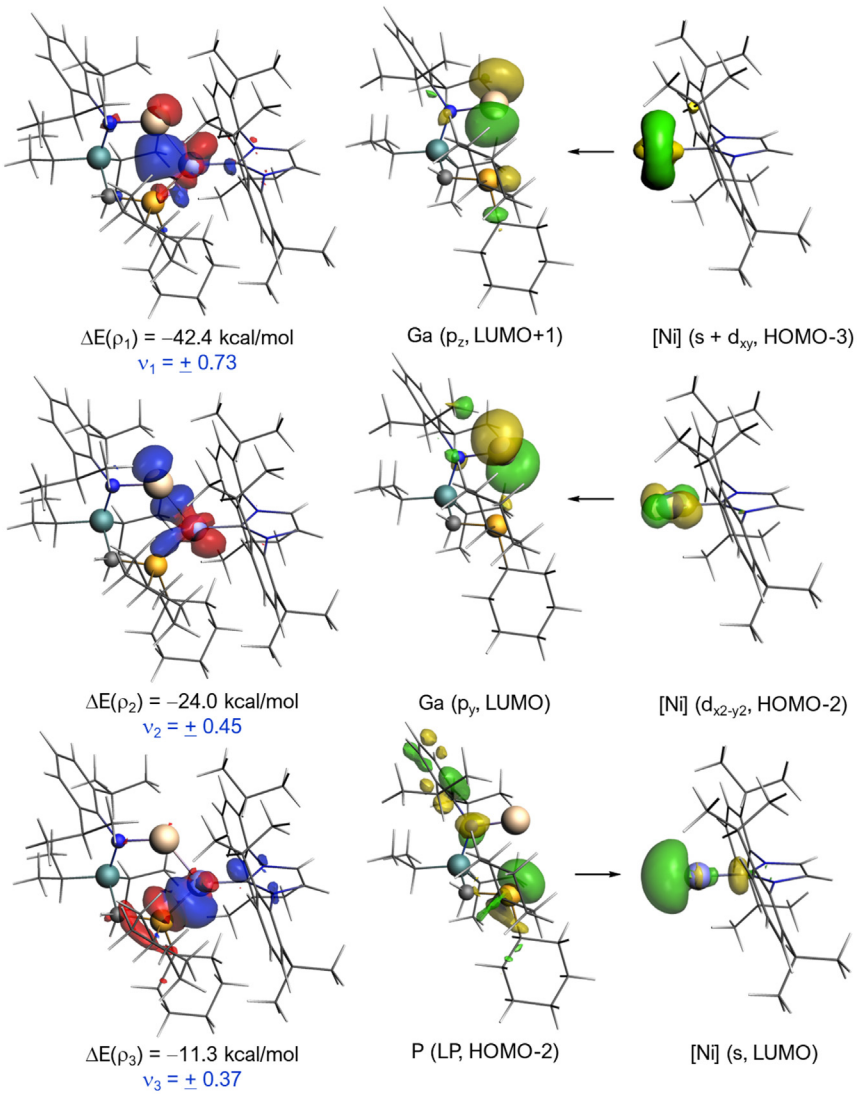

Figure 3. Contour plots of the main NOCV deformation densities ρ (isosurface value of 0.001 a.u.), associated energies ΔE(ρ), and interacting orbitals in 3

The electronic charge flows from red to blue. The eigenvalues |ν| indicate the relative size of the charge flow. All data have been computed at the ZORA-BP86-D3/TZ2P//RI-BP86-D3/def2-SVP level.

report on such a system, whereby a gallylene-ligated nickel complex can achieve temperature-dependent reversible activation of dihydrogen through hydride transfer to the electropositive gallium center. We demonstrate that this system can transfer the activated dihydrogen to alkynes, selectively generating either (*Z*)- or (*E*)-alkenes in a catalytic manner. A combination of kinetic analyses and density functional theory (DFT) investigations suggest that hydride transfer from the Ga-center to the Ni-bound alkyne is key in this process, in a sense mimicking the dual-site bimetallic mechanism at play in classical heterogeneous hydrogenation catalysts.

RESULTS AND DISCUSSION

Synthesis of a geometrically constrained Ga^{I}-Ni^{0} complex via hydrogen extrusion from a gallane

Our initial approach to Ga^{I}-ligated Ni^{0} systems looked toward the synthesis of two-coordinate gallylenes employing the phosphine-appended amido ligand, ^{Cy}L (^{Cy}L = {[$Cy_2PCH_2Si(^{i}Pr)_2$](Dipp)N}; Dipp = 2,6-$^{i}Pr_2C_6H_3$). Reduction of $^{Cy}LGaX_2$ (X = Cl, I) with a range of reducing agents led, in all cases, to over-reduction, with the formation of elemental gallium residues. We then turned our attention to a hydrogen elimination strategy, given that a few systems are known to afford complete H_2 extrusion.[39,40] Addition of $^{Cy}LGaH_2$ to IPr·Ni(η^6-tol) (IPr = [(Dipp)NC(H)]$_2$C:) led to a formal oxidative addition reaction, forming 1,2-dihydride complex **2** (Figure 2A). The molecular structure of this species reveals one terminal Ga-H ligand and one Ga···H-Ni bridging hydride ligand (Figure 2C), supported by computational analyses (Figures S129 and S130 in the supplemental information), therefore constituting a rare example of such a dihydride complex for the group 13 elements. A broad stretching band is observed in the ATR-IR (attenuated total reflectance-infrared) spectrum of **2** at ν = 1,798 cm^{-1}, which we attribute to overlapping signals for the Ga–H and Ni–H moieties. The nature of these hydride ligands is further borne out by their ^{1}H NMR (nuclear magnetic resonance) spectroscopic shifts. While these are significantly broadened at ambient temperature, they resolve into two clear sets of doublets of doublets at 213 K (Figure 2E): the signal pertaining to the terminal gallium hydride is found at δ = 5.79 ppm ($^{3}J_{HP}$ = 9.6 Hz, $^{3}J_{HH}$ = 25.0 Hz), aligning with known terminal Ga–*H* ligands,[41] and the bridging hydride at δ = –5.92 ppm ($^{2}J_{HP}$ = 78.4 Hz, $^{3}J_{HH}$ = 25.0 Hz). The latter shift is in keeping with known species bearing and E···H–Ni moiety (E = Al, Si),[42–44] though we note that no such complexes are known for gallium. We attribute signal broadening on warming to fluxional exchange processes in **2** at ambient temperature. On attempting to resolve these signals at higher temperatures, we instead observed that complex **2** spontaneously eliminates H_2 when heated. Variable temperature (VT) NMR analysis indicates an onset temperature of 50°C, where H_2 elimination is slow, while complete H_2 expulsion is observed after 40 min at 90°C (Figures S59 and S60). After this time, Ga–*H* and Ni–*H* hydride signals can no longer be observed, and a single new signal is observed in the $^{31}P\{^{1}H\}$ NMR spectrum for these mixtures. Deep red-purple crystals of the product could be isolated from

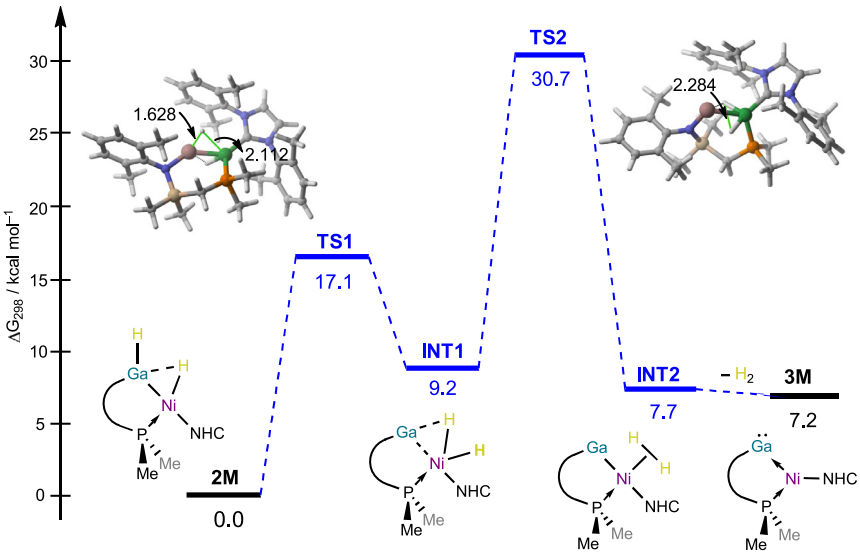

Figure 4. Computed reaction profile for the elimination of H_2 from 2M, yielding 3M

Relative free energies (ΔG, at 298 K) and bond distances are given in kcal/mol and angstroms, respectively. All data have been computed at the PCM-BP86-D3/def2-TZVPP//BP86-D3/def2-SVP level.

these reactions in up to 72% yield; a SC-XRD analysis revealed the formation of complex **3**, a highly geometrically constrained gallylene-nickel(0) complex (Figure 2D). This H_2 elimination process is related to that observed earlier by Aldridge et al. utilizing the related β-diketiminate system ^{Dip}NacnacGaH$_2$ (^{Dip}Nacnac = [C{C(Me)N(Dip)}$_2$]$^-$),[39,40] though we note that this is not a common observation, and as yet a thermally controlled example is unknown. Per complex **2**, the ^{Cy}LGa unit chelates the Ni^0 center, binding through both the P and Ga centers. This leads to a highly bent N-Ga-Ni angle of 129.78(7)°, only slightly less acute than that in **2** ($\angle_{NGaNi}$ 120.64(7)°). The Ga-Ni distances are also similar in both species (d_{GaNi}: **2** = 2.2887(9) Å; **3** = 2.2614(7) Å), indicating a minimal change in bond order on moving from gallyl to gallylene ligand. We attribute this to the chelating phosphine arm, which prevents linearization and so thwarts multiple bond formation. Here, we note that no other "bent" terminal, low-coordinate triylene-TM complexes are known. The molecular orbitals of **3** were thus investigated via computational DFT methods. We were surprised to find that, although the highest occupied molecular orbital (HOMO) is mainly located at nickel (d_{yz} atomic orbital), the HOMO−1 of this species represents a lone electron pair at Ga, and the lowest unoccupied molecular orbital (LUMO) a vacant *p*-orbital at the same center (Figures S131–S133). As such, **3** is in fact isoelectronic to a metallo-tetrylene,[45] with a Z-type gallylene ligand accepting electron density from the Lewis basic Ni^0 center.

The unprecedented nature of the bonding situation in this group 13-TM species, particularly the Ga–Ni interaction, deserves further analysis. To this end, we applied the energy decomposition analysis-natural orbital for chemical valence (EDA-NOCV) method, at the dispersion-corrected ZORA-BP86-D3/TZ2P level, to gain more insight into the main orbital interactions in **3** (Figure 3). By using the neutral [Ni(NHC)] and [Ga···P] as fragments, we found that the Ga-Ni interaction is mainly composed of two dative bonds derived from the donation of electron density from two doubly occupied *d* atomic orbitals at the transition metal to the vacant *p* atomic orbitals at gallium (denoted as ρ1 and ρ2, in Figure 3). The bonding is completed by the expected donation from the phosphine to the vacant *s* atomic orbital of the nickel atom (denoted as ρ3). Our calculations indicate that ρ1 is almost twice as strong as ρ2, with no possible backdonation from the gallium to the transition metal, which therefore agrees with the Lewis representation of **3** given in Figure 2 featuring a strong Ni→Ga dative bond and an available lone pair at the gallium center.

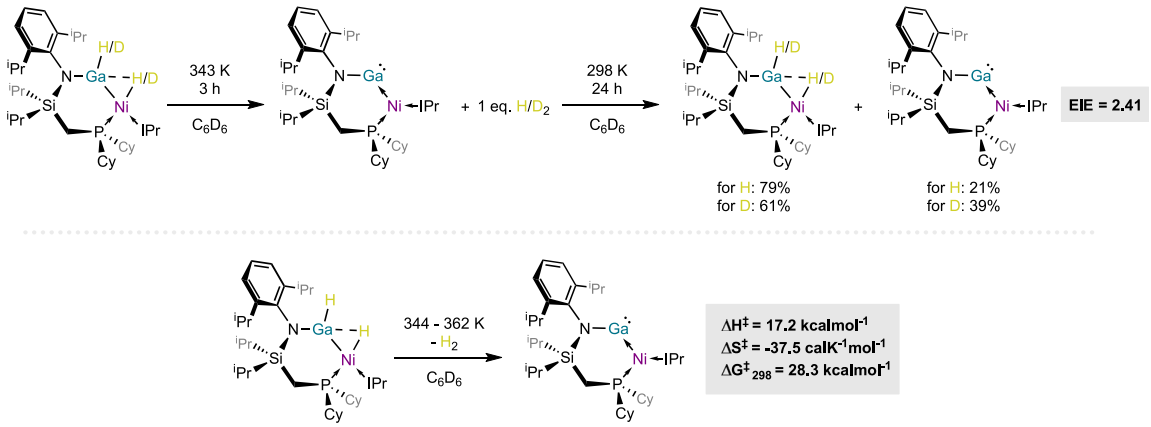

Scheme 1. Kinetic and thermodynamic studies of the reactions of 2 and 3 with alkyne and H_2/D_2, respectively

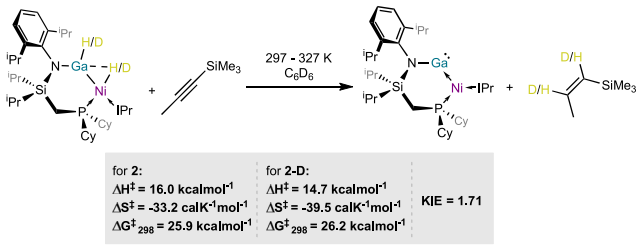

Scheme 2. Kinetic and thermodynamic studies of the reactions of 2 and 3 with alkyne and H_2/D_2, respectively

Kinetic and DFT analysis of the mechanism of H_2 elimination from 2

The mechanism for the elimination of H_2 from **2** was also investigated here (Figure 4). To this end, we investigated the process involving the model system **2M**, in which the bulky cyclohexyl and isopropyl substituents were replaced by methyl groups. The overall dihydrogen extrusion process is endergonic by 7.2 kcalmol^{-1}, with a relatively large barrier of 30.7 kcalmol^{-1}, which accounts for the observation that this process is only accessible at higher temperatures. An initial hydride migration from Ga to Ni (viz., **TS1**, $\Delta G^{\ddagger}$ = 17.1 kcalmol^{-1}) leads to nickel-dihydride complex **INT1** (ΔG_R = 9.2 kcalmol^{-1}), which is converted to Ni-H_2 complex **INT2** (ΔG_R = 7.7 kcalmol^{-1}) via a formal reductive elimination. This species readily undergoes a barrierless dissociation of H_2 in forming **3M** (ΔG_R = 7.2 kcalmol^{-1}). Notably, reductive elimination of H_2 from Ni^{II} centers is typically a challenging process. It is thus likely that the Z-type ligand character of the Ga^{I} ligand in this system aids in driving this process, as has been recently observed in zinc-coordinated nickel species.[46] Now looking at the reverse reaction, i.e., H_2 activation by **3M**, a barrier of only 23.5 kcalmol^{-1} is found, with an overall exergonic reaction profile. Given that **3** can be seen as isoelectronic to a metallo-tetrylene, which are known to undergo oxidative addition at the tetryl center,[47,48] the mechanism for H_2 binding and activation at Ga was also investigated using DFT methods (Figure S134). Although this pathway can indeed be located, the computed barrier for this process of 48.9 kcalmol^{-1} far exceeds that of the Ni-mediated pathway and would not incite facile H_2 activation at ambient temperature. Experimentally, we find that complex **3** does indeed activate H_2, under 1 atm of pressure at ambient temperature within minutes. Thus, this represents the temperature-controlled reversible activation of dihydrogen. Conducting the same reaction with D_2 gives access to the deuterated derivative of **2** (i.e., **2-D**), allowing for the determination of a room temperature primary equilibrium isotope effect (EIE) of 2.41 for the activation of H_2/D_2 by **3** (Scheme 1). Such a large normal value may suggest particularly weak Ga–H/Ni–H bonds and aids in confirming that no low-energy H_2 σ-complex is formed.[49,50] Conducting an Eyring analysis for the elimination of H_2 from **2** in the temperature range 344–362 K (Figures S65–S69) gave a $\Delta G^{\ddagger}_{298}$ value of 28.3 kcalmol^{-1}, in keeping with that for the calculated mechanism given in Figure 4, so supporting the predicted pathway.

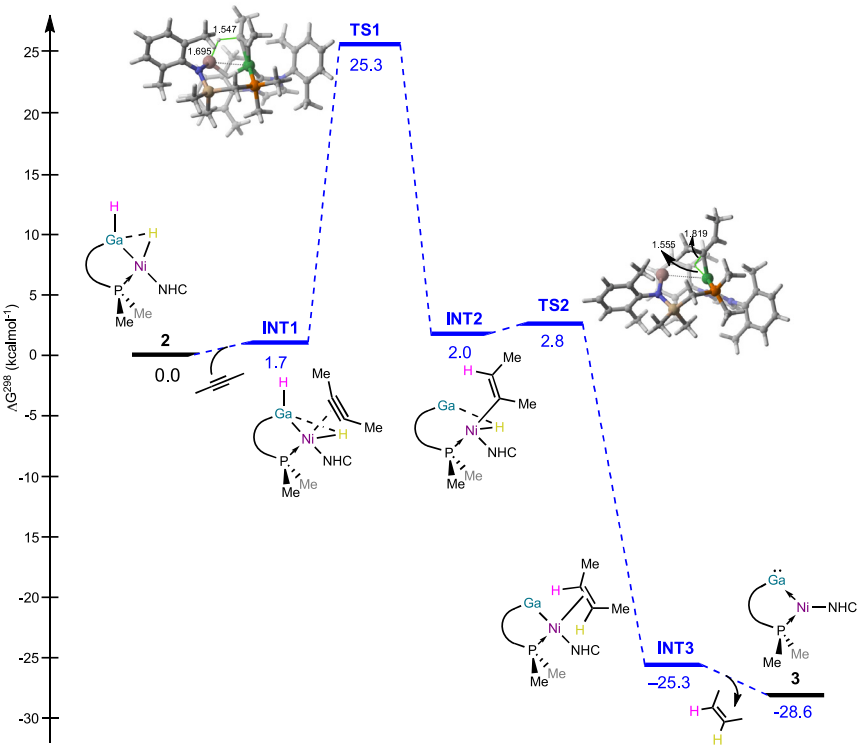

Figure 5. Computed reaction profile for the hydrogenation of 2-butyne by 2M, yielding 3M and 2-butene

Relative free energies (ΔG, at 298 K) and bond distances are given in kcal/mol and angstroms, respectively. All data have been computed at the PCM-BP86-D3/def2-TZVPP//BP86-D3/def2-SVP level.

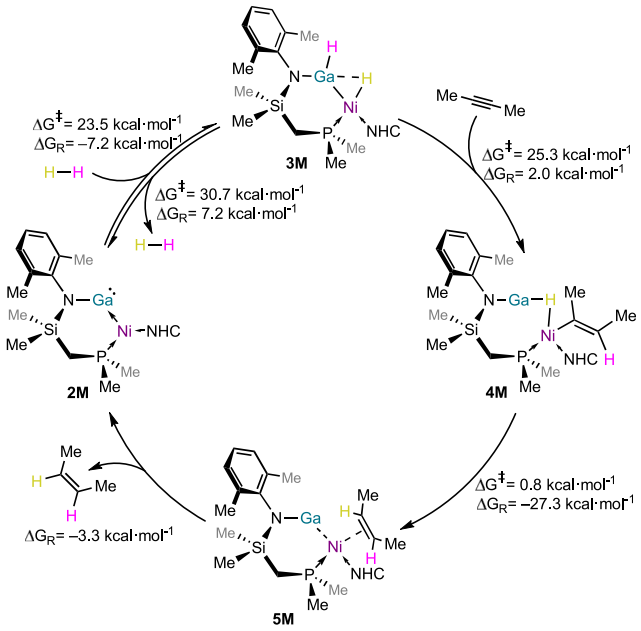

Figure 6. The proposed catalytic cycle, based on DFT calculations and supported by kinetic analyses, for the semi-hydrogenation of 2-butyne mediated by 2M

Relative free energies (at 298 K) were computed at the PCM-BP86-D3/def2-TZVPP//BP86-D3/def2-SVP level.

Experimental and computational analysis of the stoichiometric hydrogen transfer reactivity of 3

Further reactivity studies of **2** and **3** revealed that (1) hydride complex **2** can be accessed by the dehydrogenation of ammonia borane, and perhaps more importantly, (2) that **2** can be dehydrogenated by unsaturated C-C species (Scheme 2). In a first instance, a 1:1:1 mixture of **1**, [Ni(cod)$_2$], and IPr selectively leads to the formation of **3**, with cod abstracting H_2 from **2** *in situ*, borne out by the observation of cyclooctane and cyclooctene in these reaction mixtures. This represents a one-pot process for accessing gallium(I) ligands by complete dehydrogenation of a gallane. Though stoichiometric reactions of **2** with alkenes are sluggish, the addition of 4-octyne to **2** rapidly leads to the formation of **3** and *(Z)*-4-octene. In order to gain thermodynamic insights into this dehydrogenation process, an Eyring analysis was conducted. Here, we investigated the reaction of **2** with (Me_3Si)CCMe, which leads to a slower, more readily monitored reaction within the temperature range of 297 to 327 K (Scheme 2; Figures S71–S80). We find a $\Delta G^{\ddagger}_{298}$ value of 25.9 kcalmol^{-1}, in addition to $\Delta H^{\ddagger}$ and $\Delta S^{\ddagger}$ values of 16.0 kcalmol^{-1} and −33.2 calK^{-1}mol^{-1}, respectively. Of note here is the entropic factor, for which a negative value is indicative of an associative mechanism, again aligning with a rate-limiting insertion process. This is further bolstered when conducting the same study with **2-D**, which yields a slightly higher $\Delta G^{\ddagger}_{298}$ value of 26.2 kcalmol^{-1}, indicating that scission of the stronger Ga–D bond is again rate determining. Here, a primary KIE of 1.71 also aligns with a rate-limiting insertion reaction.[51,52] The mechanism for this process was further probed by DFT methods (Figures 5 and S115). First, it was found that alkyne binding at either Ni or Ga is feasible, with the former having a slightly more favorable energy (i.e., 1.8 kcalmol^{-1}) than the latter (i.e., 5.8 kcalmol^{-1}). Insertion proceeds in both cases: this leads to an "energetic sink" of −31.9 kcalmol^{-1} through binding at Ga, making this Ga-centered mechanism unfeasible. Conversely, insertion at Ni proceeds through an energetically feasible barrier of 23.6 kcalmol^{-1}, whereby the Ga–H ligand is transferred to the alkyne fragment. This, as far as we are aware, represents a unique bimetallic mechanism for alkyne hydrogenation. Finally, a small barrier of 0.8 kcalmol^{-1} is computed for the formal reductive elimination of the product alkene at Ni, leading to a π-complex. This can then readily eliminate its alkene ligand (−3.3 kcalmol^{-1}) to form **3**. Key observations here are (1) the calculated barrier to alkyne insertion, which is both rate limiting and in keeping with the magnitude of that observed experimentally, and (2) the near barrierless reductive elimination of the alkene fragment at Ni, which we again attribute to the electronic nature of the Ga ligand. Notably, the former point aids in validating the proposed mechanism to some degree, further bolstered by the calculated KIE of 1.63, which aligns with the experimentally derived value of 1.71.

Combining the calculated energetic profiles for H_2 activation and alkyne hydrogenation, one finds an overall energetically feasible reaction profile for alkyne semi-hydrogenation mediated by 2/3 (Figure 6). This mechanism explicitly involves both Ga and Ni, and as such should be considered as a cooperative process for the semi-hydrogenation of alkynes. Given the ligand-to-substrate hydride transfer mechanism, in conjunction with the constrained nature of the Ga–Ni unit in this system, one may consider this as a molecular model for established heterogeneous [GaNi] catalysts for the same catalytic process.

Alkyne semi-hydrogenation catalyzed by 2/3

Having established that (1) constrained gallylene-nickel complex **3** activates dihydrogen under mild conditions and (2) that dihydride complex **3** can transfer dihydrogen to 4-octyne to selectively generate (Z)-4-octene, we sought to explore the utility and scope of this system in alkyne semi-hydrogenation catalysis (Scheme 3). This particularly explored the selectivity for (E)/(Z)-alkene formation and the full hydrogenation to the respective alkane. First, the catalytic semi-hydrogenation of 4-octyne was optimized, leading to the following conditions: reactions are conducted in C_6D_6, with 1–2 mol % **2** or **3** as a catalyst at temperatures between 25°C and 80°C. A 0.5 bar H_2 overpressure is utilized to prevent the generation of negative pressures. This leads to complete semi-hydrogenation to (*Z*)-4-octene in 3 h at ambient temperature with 1 mol % catalyst. Conducting reactions on a slightly larger scale (i.e., using 40 mg **2**) allowed for vacuum transfer of all volatiles and isolation of the solid residue, which was confirmed by NMR spectroscopy to contain a 5:1 mixture of **2** and **3**, respectively (Figures S120 and S121 in the supplemental information). This is in keeping with **2** being the catalyst resting state, as one would expect from the kinetic and computational experiments described above. Additionally, we note that while monitoring all catalytic reactions, the only observed species is **2**, again indicative of this being the catalyst resting state.

Extending the scope for aliphatic alkynes, we found that the reaction rate and selectivity are distinctly affected by chain length, most likely due to steric pressure. 5-Decyne is selectively

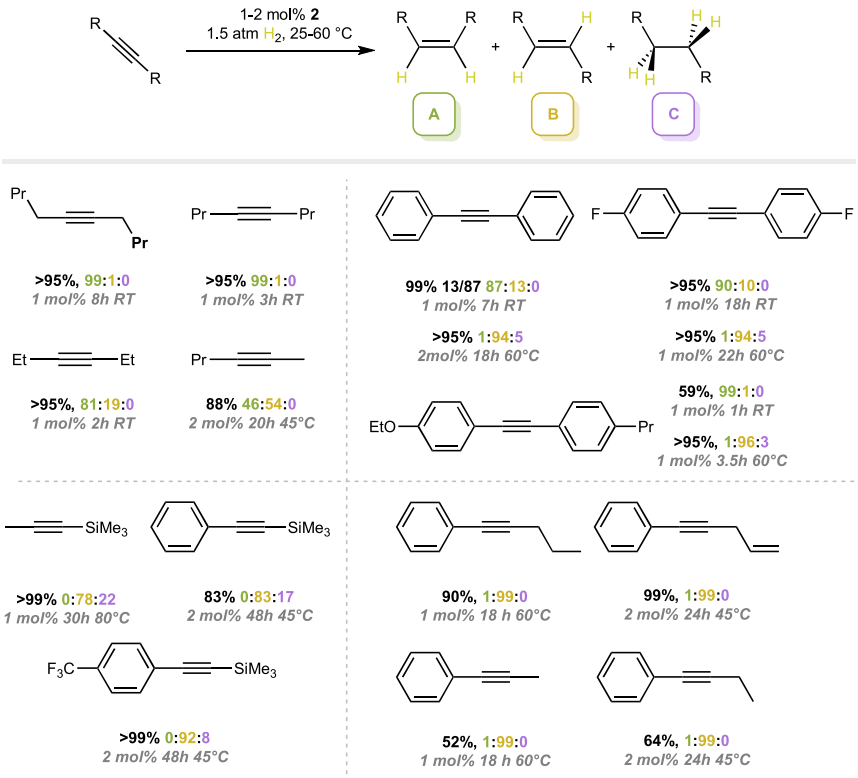

Scheme 3. Scope of the catalytic semi-hydrogenation of internal alkynes mediated by 2 or 3

All reactions employed 4 or 8 mM catalyst solutions in toluene for 1 or 2 mol % loadings, respectively, with 0.05 mmol mesitylene as an internal standard. Reactions were performed in Teflon-sealed Schlenk flasks, with stirring using a magnetic stir bar at 1,500 rpm. The given percentages relate to the conversion of the alkyne substrate to A, B, and C, and also account for by-products. All conversions are calculated by ^{1}H NMR spectroscopy, by integration against an internal standard.

semi-hydrogenated to (*Z*)-5-decene in 8 h, being significantly slower than 4-octyne, while 3-hexyne shows full conversion to 3-hexene after just 2 h, with 81% selectivity for the (*Z*)-isomer. The smaller 2-hexyne leads to near-equal mixtures of (*E*):(*Z*) isomers, implying important steric effects in limiting the rate of alkene isomerization. The (*Z*)-isomers can also be accessed for the semi-hydrogenation of bis(aryl)alkynes, albeit with some degree of (*E*)-isomer formation. Notably, however, simply increasing reaction temperature here leads to complete and selective formation of (*E*)-isomers, demonstrating control over selectivity using this catalytic system. Here, we also demonstrate the tolerance of fluoride and ether functional groups. (Aryl)(alkyl)alkynes allow only for the selective formation of (*E*)-isomers, with moderate to good conversions; however, side reactions become prominent here when employing short alkyl chains. It is interesting to note that ene-yne 1-phenyl-4-penten-1-yne selectively forms the (*Z*)-isomer of 1-phenyl-4-penten-1-ene, with no over-hydrogenation of the internal or terminal alkene observed, again demonstrating a high degree of selectivity with this catalyst. Finally, and most impressively, trimethylsilyl-substituted alkynes can also be semi-hydrogenated under the given conditions using **2** as the catalyst. This selectively leads to the formation of (*E*)-isomers, with extended reaction times and higher temperatures typically required (i.e., 30–48 h, 45°C–80°C). Nevertheless, these are among the most challenging alkynes to functionalize, highlighting the potential of the described cooperative mechanism in this catalytic system. As a whole, the catalytic efficiency of **2** and **3** compares favorably with earlier reported Ni-centered catalysts for alkyne semi-hydrogenation,[2,22,53–55] with notably mild conditions. In this light, the activity of catalysts 2/3 was also compared against their synthetic precursors, i.e., **1**, Ni(cod)$_2$, and IPr·Ni(η^6-tol) (Table S6 in the supplemental information). For this, the semi-hydrogenation of diphenylacetyene was screened, given that 2/3 can selectively generate (*Z*) or (*E*) stilbene from this alkyne depending on reaction temperature (i.e., RT or 60°C, respectively), with little observed over-hydrogenation. Both **1** and Ni(cod)$_2$ demonstrate no activity for this catalytic process, with the latter forming metallic nickel, as has been described previously.[56] IPr·Ni(η^6-tol) does show activity, with ~60% alkyne conversion observed for comparable reaction times and conditions used for full alkyne consumption employing **2**, demonstrating an enhanced activity in the latter. Further, conducting catalysis using IPr·Ni(η^6-tol) at 60°C leads to minimal isomerization (i.e., (*E*):(*Z*) ratio of 18:82), and catalyst decomposition (see the supplemental information for details). These combined control experiments would indicate that bimetallic **2** is a superior catalyst in regard to efficiency, stability, and alkene isomerization capacity.

Given that both (*Z*) and (*E*) alkenes can be accessed using **2** as a catalyst, we were curious as to the mechanism of this process, and particularly whether it involves both Ni and Ga. First, it was found that pure samples of (*Z*)-stilbene are readily and selectively isomerized to (*E*)-stilbene at 60°C in 7 h (1 mol % **2**, 1.5 bar H$_2$), with just 3% over-hydrogenation to 1,2-diphenylethane (Table S7 in the supplemental information). The mechanism of this process was then subjected to computational assessment, giving additional key insights (Figure S136 in the supplemental information). Akin to that observed for alkyne hydrogenation, the (*Z*)-alkene first coordinates at Ni, followed by Ga–*H* migration to the alkene fragment with a barrier of 30.5 kcalmol^{-1}. This is ~5 kcalmol^{-1} greater than that found for alkyne insertion, aligning with the observation that isomerization is significantly favored at higher temperatures. Following alkane rotation, rather than a classical single-center β-hydride elimination process, a dual-centered β-hydrogen abstraction reaction proceeds, mediated by gallium. This perhaps gives insights into the proficiency of this bimetallic catalyst for (*Z*)-(*E*) isomerization compared to

single-site IPr·Ni(η^6-tol), and to the best of our knowledge, represents a novel dual-centered mechanism for such a process.

Conclusions

We have described the synthesis of a low-coordinate, geometrically constrained gallylene-nickel(0) complex through complete dihydrogen extrusion from a (hydridogallyl)-nickelhydride complex, accessed through the oxidative addition of a gallane to nickel(0). This system can achieve the reversible activation of dihydrogen, which generates a highly reactive ligand-centered hydride ligand. This facilitates the semi-hydrogenation of alkynes, with hydride transfer from the gallium center being the rate-limiting step in the mechanism, as supported by in-depth kinetic and computational investigations. This gives key insights into the power of bimetallic cooperative catalysis and opens a new vista in the development of such non-innocent ligands built upon low-valent group 13 elements.

EXPERIMENTAL PROCEDURES

Syntheses for compounds **2** and **3** are given below. Full experimental information for all new compounds, catalysis studies, and kinetic studies can be found in the supplemental experimental procedures.

Synthesis and analytical data for 2

Method A

A Schlenk flask was loaded with ^{Cy}LGaH$_2$ (0.200 g, 0.349 mmol) and IPr·Ni(η^6-tol) (0.188 g, 0.349 mmol). The flask was cooled to −78°C, and toluene (20 mL) was added with rapid stirring. The reaction mixture was stirred for 30 min at this temperature, allowed to warm to ambient temperature, and stirred for a further 16 h, after which time the reaction mixture was filtered, and all volatiles removed *in vacuo*, yielding a red solid. This residue was extracted with pentane (15 mL), filtered, concentrated to ∼4 mL, and stored overnight at room temperature, resulting in the formation of large dark red crystals suitable for single-crystal X-ray diffraction analysis. The supernatant solution was removed by filtration, and the crystals were washed with small amounts of cold pentane (2 × 2 mL) and dried *in vacuo*, yielding **2** (0.273 g, 0.268 mmol, 77%) as a dark red crystalline solid.

Method B

A gas-tight Teflon-valve Schlenk flask was loaded with **3** (0.100 g, 0.098 mmol), and the solid dissolved in toluene (15 mL) at ambient temperature. The flask was subsequently pressurized with dihydrogen (5.0 grade, 1.5 bar) using 1 freeze-pump-thaw cycle, the flask was sealed, and the reaction mixture stirred for 1.5 h at room temperature. After this time, the reaction mixture was filtered, and all volatiles were removed *in vacuo*, yielding a dark red solid, which was washed with small amounts of cold pentane (2 × 5 mL) and dried *in vacuo*, yielding 72 mg of red crystalline powder. In addition, the pentane washing solution was concentrated to 5 mL and stored overnight at room temperature, leading to the formation of dark red crystals. These were isolated by filtration, washed with cold pentane (2 mL), and dried *in vacuo*, giving a combined yield of 92 mg (0.091 mmol, 93%) as a dark red crystalline solid.

^{1}H NMR (THF-d$_8$, 400 MHz, 213 K): δ = 7.52–7.47 (m, 1H, Ar-C*H*), 7.43 (t, $^3J_{HH}$ = 7.3 Hz, 2H, Ar-C*H*), 7.40–7.35 (m, 3H, Ar-C*H*), 7.31 (dd, $^3J_{HH}$ = 12.2, 7.8 Hz, 2H, Ar-C*H*), 6.91–6.84 (m, 2H, NHC-HC=CH), 6.76 (t, $^3J_{HH}$ = 7.5 Hz, 1H, Ar-C*H*), 5.79 (dd, Ga-*H*, $^3J_{HP}$/$^3J_{HH}$ = 25.0, 9.6 Hz, 1H), 4.06 (d, $^3J_{HH}$ = 9.1 Hz, 1H, iPr-C*H*), 3.38–3.27 (m, 1H, iPr-C*H*), 3.15–2.80 (m, 3H, iPr-C*H*), 2.69–2.57 (m, 1H, iPr-C*H*), 2.22 (s, 1H, Ali-C*H*), 1.84 (d, $^3J_{HH}$ = 11.3 Hz, 1H, Ali-C*H*), 1.67 (d, $^3J_{HH}$ = 9.3 Hz, 2H, Ali-C*H*), 1.60 (d, $^3J_{HH}$ = 11.5 Hz, 1H, Ali-C*H*), 1.50 (d, $^3J_{HH}$ = 6.7 Hz, 5H, Ali-C*H*), 1.40 (d, $^3J_{HH}$ = 7.9 Hz, 7H, Ali-C*H*), 1.35 (dd, $^3J_{HH}$ = 12.6, 6.5 Hz, 6H, Ali-C*H*), 1.31–1.24 (m, 5H, Ali-C*H*), 1.20 (d, $^3J_{HH}$ = 6.5 Hz, 6H, Ali-C*H*), 1.15 (d, $^3J_{HH}$ = 7.0 Hz, 6H, Ali-C*H*), 1.08 (d, J = 7.3 Hz, 7H, Ali-C*H*), 1.00–0.93 (m, 10H, Ali-C*H*), 0.84 (d, $^3J_{HH}$ = 7.6 Hz, 3H, Ali-C*H*), 0.77 (d, $^3J_{HH}$ = 7.4 Hz, 8H, Ali-C*H*), 0.41 (t, $^3J_{HH}$ = 13.6 Hz, 1H, Ali-C*H*), 0.28 (d, $^3J_{HH}$ = 7.1 Hz, 3H, Ali-C*H*), −0.36 (s, 1H, Ali-C*H*), −5.92 (dd, Ni-*H*, $^3J_{HH}$/$^2J_{HP}$ = 78.4, 25.0 Hz, 1H). **^{13}C{^{1}H} NMR** (THF-d$_8$, 101 MHz, 298 K): δ = 204.39 (d, $^3J_{PC}$ = 6.1 Hz, N-*C*-N), 149.59 (Ar-*C*), 147.37 (br, Ar-*C*), 146.70 (Ar-*C*), 145.72 (Ar-*C*), 139.48 (br, Ar-*C*), 130.30 (br, Ar-*C*), 125.58 (br, Ar-*C*), 124.95 (br, Ar-*C*), 123.37 (br, Ar-*C*), 122.26 (br, Ar-*C*), 41.65 (d, $^3J_{PC}$ = 16.9 Hz, Ali-*C*), 35.24 (Ali-*C*), 29.44 (br, Ali-*C*), 29.39 (br, Ali-*C*), 29.33 (br, Ali-*C*), 28.63 (br, Ali-*C*), 28.51 (br, Ali-*C*), 28.20 (br, Ali-*C*), 27.68 (br, Ali-*C*), 27.41 (br, Ali-*C*), 26.78 (br, Ali-*C*), 24.36 (br, Ali-*C*), 24.01 (br, Ali-*C*), 23.76 (br, Ali-*C*), 23.66 (br, Ali-*C*), 23.39 (br, Ali-*C*), 20.39 (br, Ali-*C*), 20.07 (Ali-*C*), 19.52 (Ali-*C*), 16.10 (Ali-*C*), 14.57 (Ali-*C*),6.80 (d, $^2J_{PC}$ = 9.0 Hz, Si-*C*H$_2$-P). **^{31}P{^{1}H} NMR** (THF-d$_8$, 162 MHz, 298 K): δ = 20.1 (s, CH$_2$-*P*-(Cy)$_2$).

Mass spectrometry

[LIFDI-HRMS]: [C$_{58}$H$_{89}$GaN$_3$NiPSi]$^+$: calc. 1,017.5396; exp. 1,017.5267.

Elemental analysis

C$_{58}$H$_{91}$GaN$_3$NiPSi: calc. C, 68.31% H, 9.19% N, 4.12%; found C, 68.48% H, 9.37% N, 4.12%.

IR spectroscopy $\tilde{\nu}$ [cm^{-1}]

[ATR]: 1,798 (br, Ga-H, Ni-H).

UV/vis spectroscopy λ_{max} [nm] (ε [Lmol^{-1}cm^{-1}])

340 (12,6050), 444 (27,470).

Synthesis and analytical data for 3

Method A

A Schlenk flask was loaded with Ni(cod)$_2$ (0.240 g, 0.873 mmol), dissolved in toluene (20 mL), and the solution cooled to −78°C. Subsequently, IPr was added (0.339 g, 0.873 mmol) as a solution in toluene (10 mL) over the course of 10 min. The reaction solution was then stirred for 30 min at room temperature. The resulting solution was again cooled to −78°C, and ^{Cy}LGaH$_2$ (0.500 mg, 0.698 mmol) was added as a solution in toluene (20 mL) over the course of 10 min. The reaction mixture was stirred for 10 min at −78°C, followed by 16 h at room temperature. The reaction mixture was subsequently filtered, and all volatiles were removed *in vacuo*, yielding a dark red powder. This residue was washed with pentane (10 mL) and dried *in vacuo*, yielding **3** (494 mg, 0.484 mmol) as an analytically pure dark red crystalline powder. In addition, the pentane washing solution was concentrated to 5 mL and stored at ambient temperature overnight, leading to the formation of dark red-purple crystals suitable for single-crystal X-ray diffraction analysis. These were isolated by filtration, washed with a small amount of cold pentane (2 mL), and dried *in vacuo*, yielding **3** (73 mg, 0.072 mmol). Combined yield of **3**: 567 mg (0.556 mmol, 64%).

^{1}H NMR (C$_6$D$_6$, 400 MHz, 298 K): δ = 7.21 (dd, $^3J_{HH}$ = 7.3, 5.0 Hz, 4H, NHC/N-Dipp-C*H*), 7.12 (d, $^3J_{HH}$ = 7.6 Hz, 4H, NHC/N-Dipp-C*H*), 7.06 (t, $^3J_{HH}$ = 7.5 Hz, 1H, NHC/N-Dipp-C*H*), 6.56 (s, 2H, NHC-HC=CH), 3.78 (p, $^3J_{HH}$ = 6.8 Hz, 2H, N-Dipp-iPr-C*H*), 3.23 (p, $^3J_{HH}$ = 6.8 Hz, 4H, NHC-Dipp-iPr-C*H*), 1.99–1.88 (m, 4H, Cy-C*H*), 1.80–1.75 (m, 2H, Cy-C*H*), 1.73–1.66 (m, 4H, Cy-C*H*), 1.61 (s, 2H, Cy-C*H*), 1.43 (d, $^3J_{HH}$ = 6.9 Hz, 6H, N-Dipp-iPr-C*H*$_3$), 1.38 (d, $^3J_{HH}$ = 6.8 Hz, 14H, NHC-Dipp-iPr-C*H*$_3$/iPr-C*H*), 1.28 (d, $^3J_{HH}$ = 6.6 Hz, 6H, N-Dipp-iPr-C*H*$_3$), 1.25–1.18 (m, 9H, Cy-C*H*), 1.15 (s, 1H, Cy-C*H*), 1.11 (m, 6H, iPr-C*H*$_3$), 1.03 (m, 18H, N-Dipp-iPr-C*H*$_3$/iPr-C*H*$_3$), 0.99 (m, 2H, Si-C*H*$_2$-P). **^{13}C{^{1}H} NMR** (C$_6$D$_6$, 101 MHz, 298 K): δ = 196.39 (d, $^3J_{PC}$ = 43.9 Hz, N-*C*-N), 145.88 (NHC-Dipp-$^{ipso/O}$*C*H), 145.28 (N-Dipp-$^{ipso/O}$*C*H), 144.32 (N-Dipp-$^{ipso/O}$*C*H), 138.31 (NHC-Dipp-$^{ipso/O}$*C*H), 129.37 (Dipp-^{p}CH), 124.36 (NHC-Dipp-^{m}CH), 123.22 (NHC-Dipp-^{m}CH), 122.86 (NHC-HC=CH), 121.82 (Dipp-^{p}CH), 40.96 (d, $^2J_{PC}$ = 17.1 Hz, Cy-C*H*), 34.45 (Cy-C*H*), 30.56 (d, $^4J_{PC}$ = 2.8 Hz, Cy-C*H*), 30.15 (d, $^4J_{PC}$ = 3.2 Hz, Cy-C*H*), 28.58 (NHC-Dipp-iPr-C*H*), 28.33 (Cy-C*H*), 28.23 (N-Dipp-iPr-C*H*$_3$), 28.12 (N-Dipp-iPr-C*H*), 28.01 (Cy-C*H*), 27.87 (Cy-C*H*), 26.85 (Cy-C*H*), 25.59 (Cy-C*H*), 23.60 (Cy-C*H*), 23.57 (N-Dipp-iPr-C*H*$_3$/NHC-Dipp-iPr-C*H*$_3$/iPr-CH), 22.74 (Cy-C*H*), 19.74 (iPr-C*H*$_3$), 19.30 (iPr-C*H*$_3$), 15.60 (d, $^3J_{PC}$ = 3.9 Hz), 14.30 (Cy-C*H*), 4.52 (d, $^2J_{PC}$ = 5.6 Hz, Si-CH$_2$-P). **^{31}P{^{1}H} NMR** (C$_6$D$_6$, 162 MHz, 298 K): δ = 31.1 (s, CH$_2$-*P*-(Cy)$_2$). **^{29}Si{^{1}H} NMR** (C$_6$D$_6$, 400 MHz, C$_6$D$_6$, 298 K): δ = −0.3 (d, $^2J_{SiP}$ = 6.2 Hz, CH$_2$-*Si*-(^{i}Pr)$_2$).

Mass spectrometry

[LIFDI-HRMS]: [C$_{58}$H$_{91}$GaN$_3$NiPSi]$^+$: calc. 1,017.5396 exp. 1,017.5452.

Elemental analysis

$C_{58}H_{91}GaN_3NiPSi$: calc. C, 68.44% H, 9.01% N, 4.13%; found C, 67.10% H, 9.18% N, 3.86%.

UV/vis spectroscopy λ_{max} [nm] (ε [$Lmol^{-1}cm^{-1}$])

282 (100,008), 451 (76356), and 536 (53,715).

RESOURCE AVAILABILITY

Lead contact

Further information and requests for resources should be directed to and will be fulfilled by the lead contact, Terrance J. Hadlington (terrance.hadlington@tum.de).

Materials availability

All materials generated in this study are available in the supplemental information and from the lead contact without restriction.

Data and code availability

X-ray data are available from the Cambridge Crystallographic Data Centre (CCDC) under reference numbers CCDC: 2364209 (^{CyiP}DippGaI$_2$), 2364210 (**1**), 2364211 (**2**), and 2364212 (**3**). These data can be obtained free of charge from the CCDC at https://www.ccdc.cam.ac.uk/structures/. All other experimental, spectroscopic, crystallographic, and computational data are included in the supplemental information.

ACKNOWLEDGMENTS

T.J.H. thanks the Fonds der Chemischen Industrie (FCI) for generous funding of this research through a Liebig Stipendium, the ERC for a Starting grant (project 101076897—SINGAMBI), the Technical University Munich for the generous endowment of TUM Junior Fellow funds, and Prof. Fässler for his continued support. T.L.K. thanks the FCI for the generous endowment of a Kekulé Stipendium. I.F. is grateful for financial support from grants PID2022-139318NB-I00 and RED2022-134331-T funded by MICIU/AEI/10.13039/501100011033. We also thank P. Mollik and J. Gilch for their help in acquiring LIFDI-MS data and J. Stephan for help in acquiring ATR-IR data.

AUTHOR CONTRIBUTIONS

T.L.K. carried out all experimental work and analysis. I.F. conducted all computational work and prepared the computational part of the manuscript. T.J.H. conceived and supervised the project and prepared the manuscript.

DECLARATION OF INTERESTS

The authors declare no competing interests.

SUPPLEMENTAL INFORMATION

Supplemental information can be found online at https://doi.org/10.1016/j.chempr.2024.10.016.

Received: July 11, 2024
Revised: September 12, 2024
Accepted: October 22, 2024
Published: November 13, 2024

REFERENCES

1. J.G. De Vries and C.J. Elsevier, eds. (2006). The Handbook of Homogeneous Hydrogenation, First Edition (Wiley).
2. Gregori, B.J., Schmotz, M.W.S., and Jacobi Von Wangelin, A. (2022). Stereoselective Semi-Hydrogenations of Alkynes by First-Row (3d) Transition Metal Catalysts. ChemCatChem *14*, e202200886. https://doi.org/10.1002/cctc.202200886.
3. Zhang, L., Zhou, M., Wang, A., and Zhang, T. (2020). Selective Hydrogenation over Supported Metal Catalysts: From Nanoparticles to Single Atoms. Chem. Rev. *120*, 683–733. https://doi.org/10.1021/acs.chemrev.9b00230.
4. Deng, X., Wang, J., Guan, N., and Li, L. (2022). Catalysts and mechanisms for the selective heterogeneous hydrogenation of carbon-carbon triple bonds. Cell Rep. Phys. Sci. *3*, 101017. https://doi.org/10.1016/j.xcrp.2022.101017.
5. Lindlar, H. (1952). Ein neuer Katalysator für selektive Hydrierungen. Helv. Chim. Acta *35*, 446–450. https://doi.org/10.1002/hlca.19520350205.
6. Teschner, D., Révay, Z., Borsodi, J., Hävecker, M., Knop-Gericke, A., Schlögl, R., Milroy, D., Jackson, S.D., Torres, D., and Sautet, P. (2008). Understanding Palladium Hydrogenation Catalysts: When the Nature of the Reactive Molecule Controls the Nature of the Catalyst Active Phase. Angew. Chem. Int. Ed. Engl. *47*, 9274–9278. https://doi.org/10.1002/anie.200802134.
7. Hamm, G., Schmidt, T., Breitbach, J., Franke, D., Becker, C., and Wandelt, K. (2009). The Adsorption of Ethene on Pd(111) and Ordered Sn/Pd(111) Surface Alloys. Z. Phys. Chem. *223*, 209–232. https://doi.org/10.1524/zpch.2009.6033.
8. Armbrüster, M., Kovnir, K., Friedrich, M., Teschner, D., Wowsnick, G., Hahne, M., Gille, P., Szentmiklósi, L., Feuerbacher, M., Heggen, M., et al. (2012). Al13Fe4 as a low-cost alternative for palladium in heterogeneous hydrogenation. Nat. Mater. *11*, 690–693. https://doi.org/10.1038/nmat3347.
9. Wang, L., Li, F., Chen, Y., and Chen, J. (2019). Selective hydrogenation of acetylene on SiO2-supported Ni-Ga alloy and intermetallic compound. J. Energy Chem. *29*, 40–49. https://doi.org/10.1016/j.jechem.2018.02.001.
10. Liu, H., Chen, X., Liu, S., Du, Y., Zhu, W., Hu, Z., Armbrüster, M., and Liang, C. (2024). Catalysts Derived from Al–Ni Intermetallic Compounds for Efficient Selective Semihydrogenation of Phenylacetylene. Ind. Eng. Chem. Res. *63*, 3608–3620. https://doi.org/10.1021/acs.iecr.3c04134.
11. Horiuti, I., and Polanyi, M. (1934). Exchange reactions of hydrogen on metallic catalysts. Trans. Faraday Soc. *30*, 1164. https://doi.org/10.1039/tf9343001164.
12. Vilé, G., Baudouin, D., Remediakis, I.N., Copéret, C., López, N., and Pérez-Ramírez, J. (2013). Silver Nanoparticles for Olefin Production: New Insights into the Mechanistic Description of Propyne Hydrogenation. ChemCatChem *5*, 3750–3759. https://doi.org/10.1002/cctc.201300569.
13. Yan, H., Cheng, H., Yi, H., Lin, Y., Yao, T., Wang, C., Li, J., Wei, S., and Lu, J. (2015). Single-Atom Pd $_1$ /Graphene Catalyst Achieved by Atomic Layer Deposition: Remarkable Performance in Selective Hydrogenation of 1,3-Butadiene. J. Am. Chem. Soc. *137*, 10484–10487. https://doi.org/10.1021/jacs.5b06485.
14. Liu, P., Zhao, Y., Qin, R., Mo, S., Chen, G., Gu, L., Chevrier, D.M., Zhang, P., Guo, Q., Zang, D., et al. (2016). Photochemical route for synthesizing atomically dispersed palladium catalysts. Science *352*, 797–801. https://doi.org/10.1126/science.aaf5251.
15. Karunananda, M.K., and Mankad, N.P. (2015). *E* -Selective Semi-Hydrogenation of Alkynes by Heterobimetallic Catalysis. J. Am. Chem. Soc. *137*, 14598–14601. https://doi.org/10.1021/jacs.5b10357.
16. Zhang, Y., Karunananda, M.K., Yu, H.-C., Clark, K.J., Williams, W., Mankad, N.P., and Ess, D.H. (2019). Dynamically Bifurcating Hydride Transfer Mechanism and Origin of Inverse Isotope Effect for Heterodinuclear AgRu-Catalyzed Alkyne Semihydrogenation. ACS Catal. *9*, 2657–2663. https://doi.org/10.1021/acscatal.8b04130.
17. Van Beek, C.B., Killian, L., Lutz, M., Weingarth, M., Asundi, A.S., Sarangi, R., Klein Gebbink, R.J.M., and Broere, D.L.J. (2022). *E* -selective Semi-hydrogenation of Alkynes under Mild Conditions by a Diruthenium Hydride Complex. Chemistry *28*, e202202527. https://doi.org/10.1002/chem.202202527.

18. Takemoto, S., Kitamura, M., Saruwatari, S., Isono, A., Takada, Y., Nishimori, R., Tsujiwaki, M., Sakaue, N., and Matsuzaka, H. (2019). Bis(bipyridine) ruthenium(ii) bis(phosphido) metalloligand: synthesis of heterometallic complexes and application to catalytic (E)-selective alkyne semi-hydrogenation. Dalton Trans. *48*, 1161–1165. https://doi.org/10.1039/C8DT04646H.

19. Desai, S.P., Ye, J., Zheng, J., Ferrandon, M.S., Webber, T.E., Platero-Prats, A.E., Duan, J., Garcia-Holley, P., Camaioni, D.M., Chapman, K.W., et al. (2018). Well-Defined Rhodium–Gallium Catalytic Sites in a Metal–Organic Framework: Promoter-Controlled Selectivity in Alkyne Semihydrogenation to *E* -Alkenes. J. Am. Chem. Soc. *140*, 15309–15318. https://doi.org/10.1021/jacs.8b08550.

20. Desai, S.P., Ye, J., Islamoglu, T., Farha, O.K., and Lu, C.C. (2019). Mechanistic Study on the Origin of the *Trans* Selectivity in Alkyne Semihydrogenation by a Heterobimetallic Rhodium–Gallium Catalyst in a Metal–Organic Framework. Organometallics *38*, 3466–3473. https://doi.org/10.1021/acs.organomet.9b00331.

21. Maity, R., Birenheide, B.S., Breher, F., and Sarkar, B. (2021). Cooperative Effects in Multimetallic Complexes Applied in Catalysis. ChemCatChem *13*, 2337–2370. https://doi.org/10.1002/cctc.202001951.

22. Ramirez, B.L., and Lu, C.C. (2020). Rare-Earth Supported Nickel Catalysts for Alkyne Semihydrogenation: Chemo- and Regioselectivity Impacted by the Lewis Acidity and Size of the Support. J. Am. Chem. Soc. *142*, 5396–5407. https://doi.org/10.1021/jacs.0c00905.

23. Alig, L., Fritz, M., and Schneider, S. (2019). First-Row Transition Metal (De)Hydrogenation Catalysis Based On Functional Pincer Ligands. Chem. Rev. *119*, 2681–2751. https://doi.org/10.1021/acs.chemrev.8b00555.

24. Ludwig, J.R., and Schindler, C.S. (2017). Catalyst: Sustainable Catalysis. Chem *2*, 313–316. https://doi.org/10.1016/j.chempr.2017.02.014.

25. Van Der Vlugt, J.I. (2012). Cooperative Catalysis with First-Row Late Transition Metals. Eur. J. Inorg. Chem. *2012*, 363–375. https://doi.org/10.1002/ejic.201100752.

26. Khusnutdinova, J.R., and Milstein, D. (2015). Metal–Ligand Cooperation. Angew. Chem. Int. Ed. Engl. *54*, 12236–12273. https://doi.org/10.1002/anie.201503873.

27. Stevens, M.A., and Colebatch, A.L. (2022). Cooperative approaches in catalytic hydrogenation and dehydrogenation. Chem. Soc. Rev. *51*, 1881–1898. https://doi.org/10.1039/D1CS01171E.

28. Shimbayashi, T., and Fujita, K. (2020). Recent Advances in Homogeneous Catalysis via Metal–Ligand Cooperation Involving Aromatization and Dearomatization. Catalysts *10*, 635. https://doi.org/10.3390/catal10060635.

29. Ye, J., Cammarota, R.C., Xie, J., Vollmer, M.V., Truhlar, D.G., Cramer, C.J., Lu, C.C., and Gagliardi, L. (2018). Rationalizing the Reactivity of Bimetallic Molecular Catalysts for CO $_2$ Hydrogenation. ACS Catal. *8*, 4955–4968. https://doi.org/10.1021/acscatal.8b00803.

30. Vollmer, M.V., Ye, J., Linehan, J.C., Graziano, B.J., Preston, A., Wiedner, E.S., and Lu, C.C. (2020). Cobalt-Group 13 Complexes Catalyze CO 2 Hydrogenation via a Co(−I)/Co(I) Redox Cycle. ACS Catal. *10*, 2459–2470. https://doi.org/10.1021/acscatal.9b03534.

31. Harman, W.H., and Peters, J.C. (2012). Reversible H $_2$ Addition across a Nickel–Borane Unit as a Promising Strategy for Catalysis. J. Am. Chem. Soc. *134*, 5080–5082. https://doi.org/10.1021/ja211419t.

32. MacMillan, S.N., Hill Harman, W., and Peters, J.C. (2014). Facile Si–H bond activation and hydrosilylation catalysis mediated by a nickel–borane complex. Chem. Sci. *5*, 590–597. https://doi.org/10.1039/C3SC52626G.

33. Lin, T.-P., and Peters, J.C. (2013). Boryl-Mediated Reversible H $_2$ Activation at Cobalt: Catalytic Hydrogenation, Dehydrogenation, and Transfer Hydrogenation. J. Am. Chem. Soc. *135*, 15310–15313. https://doi.org/10.1021/ja408397v.

34. Gorgas, N., Stadler, B., White, A.J.P., and Crimmin, M.R. (2024). Vinylic C–H Activation of Styrenes by an Iron–Aluminum Complex. J. Am. Chem. Soc. *146*, 4252–4259. https://doi.org/10.1021/jacs.3c14281.

35. Stadler, B., Gorgas, N., White, A.J.P., and Crimmin, M.R. (2023). Double Deprotonation of CH $_3$ CN by an Iron-Aluminium Complex**. Angew. Chem. Int. Ed. Engl. *62*, e202219212. https://doi.org/10.1002/anie.202219212.

36. Gorgas, N., White, A.J.P., and Crimmin, M.R. (2022). Cooperative C–H Bond Activation by a Low-Spin d 6 Iron–Aluminum Complex. J. Am. Chem. Soc. *144*, 8770–8777. https://doi.org/10.1021/jacs.2c02662.

37. Ward, R.J., Rungthanaphatsophon, P., Huang, P., Kelley, S.P., and Walensky, J.R. (2023). Cooperative dihydrogen activation with unsupported uranium–metal bonds and characterization of a terminal U(iv) hydride. Chem. Sci. *14*, 12255–12263. https://doi.org/10.1039/D3SC04857H.

38. Muhr, M., Liang, H., Allmendinger, L., Bühler, R., Napoli, F.E., Ukaj, D., Cokoja, M., Jandl, C., Kahlal, S., Saillard, J.Y., et al. (2023). Catalytic Alkyne Semihydrogenation with Polyhydride Ni/Ga Clusters. Angew. Chem. Int. Ed. Engl. *62*, e202308790. https://doi.org/10.1002/anie.202308790.

39. Abdalla, J.A.B., Caise, A., Sindlinger, C.P., Tirfoin, R., Thompson, A.L., Edwards, A.J., and Aldridge, S. (2017). Structural snapshots of concerted double E–H bond activation at a transition metal centre. Nat. Chem. *9*, 1256–1262. https://doi.org/10.1038/nchem.2792.

40. Turner, J., Abdalla, J.A.B., Bates, J.I., Tirfoin, R., Kelly, M.J., Phillips, N., and Aldridge, S. (2013). Formation of sub-valent carbenoid ligands by metal-mediated dehydrogenation chemistry: coordination and activation of H2Ga{(NDippCMe)2CH}. Chem. Sci. *4*, 4245. https://doi.org/10.1039/c3sc52133h.

41. Cowley, A.H., Gabbaï, F.P., Isom, H.S., Carrano, C.J., and Bond, M.R. (1994). Base-Free Monomeric Organogallium Hydrides. Angew. Chem. Int. Ed. Engl. *33*, 1253–1255. https://doi.org/10.1002/anie.199412531.

42. Steinke, T., Gemel, C., Cokoja, M., Winter, M., and Fischer, R.A. (2004). AlCp* as a Directing Ligandligand: C–H and Si–H bond activation at the reactive intermediate [Ni(AlCp*)(3)]. Angew. Chem. Int. Ed. Engl. *43*, 2299–2302. https://doi.org/10.1002/anie.200353114.

43. Witzke, R.J., and Tilley, T.D. (2019). A two-coordinate Ni(i) silyl complex: CO $_2$ insertion and oxidatively-induced silyl migrations. Chem. Commun. *55*, 6559–6562. https://doi.org/10.1039/C9CC03128F.

44. Schmidt, D., Zell, T., Schaub, T., and Radius, U. (2014). Si–H bond activation at {(NHC)2Ni0} leading to hydrido silyl and bis(silyl) complexes: a versatile tool for catalytic Si–H/D exchange, acceptorless dehydrogenative coupling of hydrosilanes, and hydrogenation of disilanes to hydrosilanes. Dalton Trans. *43*, 10816–10827. https://doi.org/10.1039/c4dt01250j.

45. Somerville, R.J., and Campos, J. (2021). Cooperativity in Transition Metal Tetrylene Complexes. Eur. J. Inorg. Chem. *2021*, 3488–3498. https://doi.org/10.1002/ejic.202100460.

46. Zhang, T., Zhong, K., Lin, Z.-K., Niu, L., Li, Z.-Q., Bai, R., Engle, K.M., and Lan, Y. (2023). Revised Mechanism of C(sp3)-C(sp3) Reductive Elimination from Ni(II) with the Assistance of a Z-Type Metalloligand. J. Am. Chem. Soc. *145*, 2207–2218. https://doi.org/10.1021/jacs.2c09739.

47. Inomata, K., Watanabe, T., Miyazaki, Y., and Tobita, H. (2015). Insertion of a Cationic Metallogermylene into E–H Bonds (E = H, B, Si). J. Am. Chem. Soc. *137*, 11935–11937. https://doi.org/10.1021/jacs.5b08169.

48. Juckel, M.M., Hicks, J., Jiang, D., Zhao, L., Frenking, G., and Jones, C. (2017). An acyclic zincagermylene: rapid activation of dihydrogen at sub-ambient temperature. Chem. Commun. *53*, 12692–12695. https://doi.org/10.1039/C7CC08430G.

49. Zhu, G., Janak, K.E., and Parkin, G. (2006). A normal equilibrium isotope effect for oxidative addition of H $_2$ to (η6 -anthracene)Mo(PMe $_3$) $_3$. Chem. Commun. *23*, 2501–2503. https://doi.org/10.1039/B604159K.

50. Parkin, G. (2007). Applications of deuterium isotope effects for probing aspects of reactions involving oxidative addition and reductive elimination of H–H and C–H bonds. Label. Comp. Radiopharmac. *50*, 1088–1114. https://doi.org/10.1002/jlcr.1435.

51. Doherty, N.M., and Bercaw, J.E. (1985). Kinetics and mechanism of the insertion of olefins into transition metal-hydride bonds. J. Am. Chem. Soc. *107*, 2670–2682. https://doi.org/10.1021/ja00295a020.

52. Gómez-Gallego, M., and Sierra, M.A. (2011). Kinetic Isotope Effects in the Study of Organometallic Reaction Mechanisms. Chem. Rev. *111*, 4857–4963. https://doi.org/10.1021/cr100436k.

53. Thiel, N.O., Kaewmee, B., Tran Ngoc, T., and Teichert, J.F. (2020). A Simple Nickel Catalyst Enabling an *E* -Selective Alkyne Semihydrogenation. Chemistry *26*, 1597–1603. https://doi.org/10.1002/chem.201903850.

54. Farrar-Tobar, R.A., Weber, S., Csendes, Z., Ammaturo, A., Fleissner, S., Hoffmann, H., Veiros, L.F., and Kirchner, K. (2022). *E* -Selective Manganese-Catalyzed Semihydrogenation of Alkynes with H_2 Directly Employed or In Situ-Generated. ACS Catal. *12*, 2253–2260. https://doi.org/10.1021/acscatal.1c06022.

55. Murugesan, K., Bheeter, C.B., Linnebank, P.R., Spannenberg, A., Reek, J.N.H., Jagadeesh, R.V., and Beller, M. (2019). Nickel-Catalyzed Stereodivergent Synthesis of *E* - and *Z* -Alkenes by Hydrogenation of Alkynes. ChemSusChem *12*, 3363–3369. https://doi.org/10.1002/cssc.201900784.

56. Rodríguez, A.A., Garduño, J.A., and García, J.J. (2020). Nickel(ii) and nickel(0) complexes as precursors of nickel nanoparticles for the catalytic hydrogenation of benzonitrile. New J. Chem. *44*, 1082–1089. https://doi.org/10.1039/C9NJ05221F.